OPTICA

Backward jet propulsion of particles by femtosecond pulses in hollow-core photonic crystal fiber

Maria N. Romodina,* Shangran Xie, Francesco Tani, and Philip St.J. Russell

Max Planck Institute for the Science of Light, Staudtstr. 2, 91058 Erlangen, Germany
**Corresponding author: maria.romodina@mpl.mpg.de*

Received 28 July 2021; revised 16 January 2022; accepted 24 January 2022; published 24 February 2022

A dielectric microparticle, optically trapped within an air-filled hollow-core photonic crystal fiber (PCF), is accelerated backwards close to the speed of sound when a single guided femtosecond pulse is incident upon it. Acting as a spherical lens, the particle focuses a fraction of the pulse energy onto its inner rear surface, causing the material to ablate. The resulting plasma and vapor jet act like a rocket motor, driving the particle backward at peak accelerations conservatively estimated at more than a million times gravity. Using counter-propagating pulses to suppress particle motion, the effect may permit the inner core walls to be coated locally with different materials, allowing optical devices to be created at otherwise inaccessible points inside long lengths of hollow-core PCF.

https://doi.org/10.1364/OPTICA.439087

1. INTRODUCTION

Since its invention by Ashkin in 1970 [1], tweezering and manipulation of small particles using focused laser beams has become a powerful tool with a broad range of applications in biology and physics [2]. With the advent of low-loss hollow-core photonic crystal fiber (HC-PCF), it is possible to trap particles transversely by gradient forces and transport them over long distances by radiation pressure [3]. Such "flying particles" have been proposed as reconfigurable point sensors [4], and the hollow-core system itself represents convenient means of monitoring airborne PM2.5 particles [5]. An optically trapped microsphere can also act as ball lens, focusing incident light to a tight spot. This has been used to enhance the resolution of two-photon photopolymerization printing [6] and femtosecond laser machining of glass [7,8]. By appropriate choice of parameters, a femtosecond pulse can be focused to a spot within the tweezered particle itself, causing ablation and a permanent change in shape [9,10]; in such experiments, the particle typically jumps out of the trap and is lost, making further investigation difficult. Here, we report about the interaction between femtosecond optical pulses and a particle transversely trapped within a HC-PCF, but free to move along the fiber axis. The initial aim of this work was to explore the ablation or evaporation of a trapped particle as a means of coating the inside surfaces of HC-PCF locally with different materials, which would open up the possibility of creating devices such as lasers, amplifiers, and Bragg gratings at inaccessible points within a long length of HC-PCF. While conducting the experiments, we observed intriguing rocket-like backward motion, at initial speeds approaching the speed of sound, of the silica particles (diameter, 0.8–4 μm) after incidence of a single femtosecond pulse [Fig. 1(a)]. As we will see, this is caused by the formation of a short-lived ablation jet at the rear surface of the particle. The hollow-core system uniquely allows post-ablation dynamics to be precisely studied within a well-controlled micro-environment.

2. EXPERIMENT

In the experiments, we used an anti-resonant-reflecting "single-ring" HC-PCF [11] with a core diameter $D = 29.4$ μm [see the scanning electron micrograph in Fig. 1(a)]. For trapping, a continuous wave laser beam at 1064 nm was split in two parts with a variable power ratio and launched into opposite ends of the fiber. The axial particle position could then be adjusted by suitably controlling the splitting ratio. An electronic shutter was used to create short bursts of (one or more) femtosecond pulses from a laser delivering 40 fs few-μJ pulses at the wavelength 800 nm and the repetition rate 100 Hz. These were then launched unidirectionally into the fiber. The motion of the trapped particle was monitored through from the side using a fast CMOS video camera (maximum frame rate 225 kHz). After the arrival of each fs pulse, the particle moved backwards into the path of the incoming pulse train, as can be seen in the sequence of video frames in the inset of Fig. 1(b).

For diameter-to-wavelength ratios (d/λ) within a suitable range, the microsphere, acting as a ball lens, focuses light to a spot just within its output surface, causing ablation if the intensity is high enough. To explore this in more detail, we used finite element modelling (see Supplement 1) to calculate the field intensity distribution for different values of d/λ (Fig. 2). The optimal value turns out to be around $d/\lambda = 2/0.8 = 2.5$, under which circumstances the incident intensity is enhanced by a factor of ~30 just within the

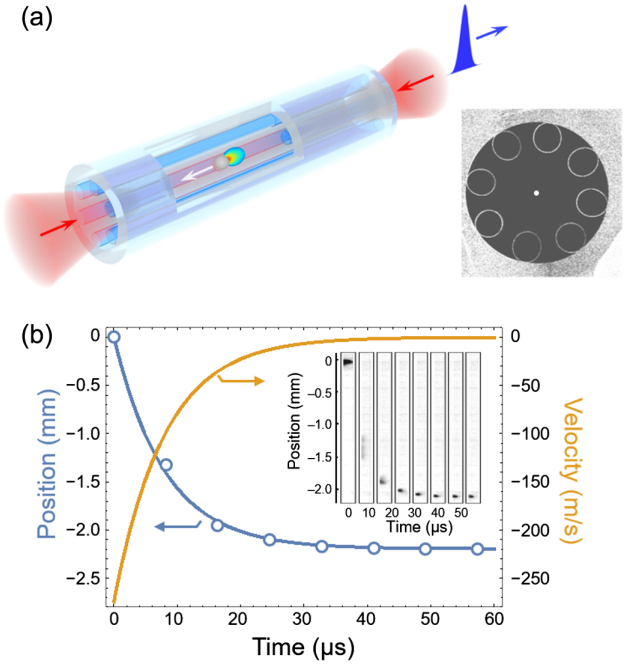

Fig. 1. Schematic and measurements of the rocket motion of optically trapped particles. (a) Sketch of the experiment. A particle is trapped inside a HC-PCF by two counter-propagating CW laser beams (red). Femtosecond pulses (blue) are launched unidirectionally into the fiber, causing ablation at the rear side of the particle. On the lower right is a scanning electron micrograph of the single-ring PCF microstructure used in the experiments (core diameter 29.4 μm). The white dot in the center represents the particle used in (b) (drawn to scale). (b) Position as a function of time for a particle 1.76 μm in diameter, taken from successive video camera frames (inset) after interaction with a single femtosecond pulse of energy $E_0 = 4.47$ μJ. In the second frame, the particle was moving too quickly to be captured clearly by the camera. The fitting parameters [see Eq. (1)] $v_0 = -274$ m/s and $\gamma = 0.125$ μs^{-1} were used to obtain the curves.

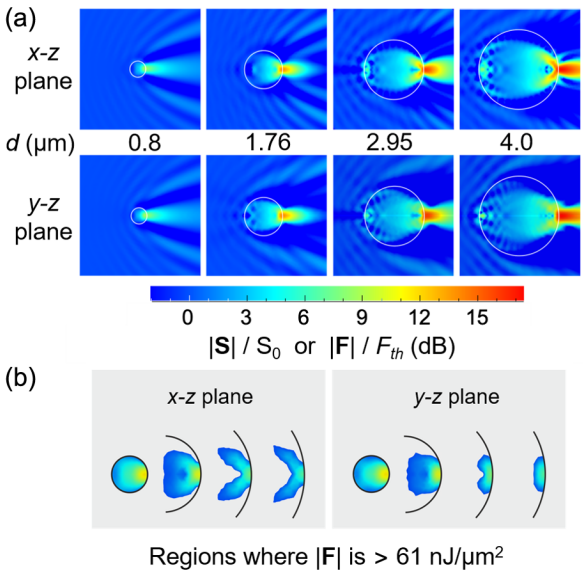

Fig. 2. Lensing effect for different silica (refractive index, 1.45) particle diameters. (a) Numerically calculated plots of the modulus of the local Poynting vector $|S|$ (W/m^2), normalized to its value S_0 in the incident plane wave (wavelength 800 nm, x-polarized). See Supplement 1 for details. At the focus, the maximum flux enhancement in the glass is 7.5, 30, 45, and 60 times for $d = 0.8$, 1.76, 2.95, and 4.0 μm, respectively. (b) Maps of the regions where $|\mathbf{F}| > F_{\text{th}} = 61$ nJ/μm^2 for the four particle sizes in (a) (left to right), keeping the energy incident on the particles constant at $f_E E_0 = 62.4$ nJ. The value of F_{th}, which is used as the reference in the dB scale, was chosen to yield the best fit between numerical modelling and experiment (see Supplement 1).

rear surface of the microsphere. If the pulse energy is high enough for the local energy fluence (nJ/μ^2) to be above the threshold for glass ionization [12], a hypersonic plasma plume forms, resulting in momentum transfer to the particle, which is abruptly accelerated to a high backward velocity, followed by an exponential velocity drop caused by viscous drag, and ending with the particle coming to a halt at a new position. After 10 ms, a second pulse arrives, and the particle once again jumps backwards. Provided the pulse energy is not so high as to cause rapid shattering, the particle remains trapped in the core even after the exposure to many pulses.

3. THEORY

If v_0 is the initial particle velocity at time $t = 0$ following the action of a single pulse, the subsequent position z and velocity v are given by

$$z(t) = v_0(1 - e^{-\gamma t})/\gamma, \quad v(t) = v_0 e^{-\gamma t}, \tag{1}$$

where $\gamma = 18\eta/(\rho d^2 C)$, η is the dynamic viscosity of air, C the slip correction factor [13], and ρ the density of fused silica (2196 kg.m^{-3}).

The energy per unit area (fluence) at core center in the absence of a particle is $F_0 = 4E_0/(\pi D^2 J_1^2(u_{01}))$, where E_0 is the energy in the laser pulse, J_n is n-order Bessel function, and u_{01} is the first zero of J_0. Since $d/D \ll 1$, F_0 is almost identical to the energy fluence incident on the particle, so that the fraction of the pulse energy intercepted by the particle is $f_E = (d/D)^2/J_1^2(u_{01})$. Applying conservation of energy and momentum, we can relate the velocity v_a and mass m_a of the ablated material, yielding

$$\frac{v_a}{v_0} = 1 - \frac{m_0}{m_a} = -\frac{2 f_k f_E E_0}{m_0 v_0^2}, \tag{2}$$

where f_k is the fraction of the available energy converted to kinetic energy (see below for discussion), and m_0 is the initial mass of the particle. The ablation velocity v_a can be independently estimated by assuming all the energy released by glass ionization goes to kinetic energy in the particle and the ablated material. This allows us to write [14]

$$m_a v_a^2 + (m_0 - m_a) v_0^2 = 2U n_e m_a/\rho, \tag{3}$$

where U is the energy bandgap of silica (9 eV) and n_e the electron density (2.1×10^{28} m^{-3}). Applying momentum conservation, and noting that $m_a/m_0 \ll 1$ and $v_a/v_0 \gg 1$, we obtain

$$v_a \simeq \sqrt{2U n_e/\rho} = 5.25 \text{ km/s}. \tag{4}$$

4. RESULTS

Figure 1(b) shows positional data taken from successive video frames for a particle of diameter 1.76 μm and a launched pulse energy $E_0 = 4.47$ μJ, corresponding to $f_E E_0 = 59$ nJ and $F_0 = 24.4$ nJ/μm^2. Only eight data-points could be measured, owing to the high particle velocity and the limited framerate of the video camera. After fitting to Eq. (1), we find $v_0 = -274$ m.s^{-1},

$\gamma = 0.125\ \mu s^{-1}$, and $\eta/C = 4.72 \times 10^{-5}$ Pa.s. Entering $v_a = 5.25$ km/s into Eq. (2) then yields $m_a = 0.32$ femtogram or 5% of m_0, and $f_k = 0.079$. The particle was accelerated to $v_0 = -274$ m.s^{-1} over a time shorter than 10 μs, suggesting a peak acceleration more than a million times gravity.

In Fig. 3(a), the dependence of v_0 on the energy incident on the particle is plotted for three different particle diameters. In Fig. 3(b), the same data are used to plot the kinetic energy conversion factor f_k versus $f_E E_0$. For a particle that is 2.95 μm in diameter and a launched pulse energy of 1.68 μJ, $f_E E_0 = 62.4$ nJ, the measured initial velocity was $v_0 = -73.1$ m/s [points enclosed with red squares in Figs. 3(a) and 3(b)]. By entering these values, together with $v_a = 5.25$ km/s into Eq. (3), we find $m_a = 0.405$ femtogram or 1.37% of m_0, and $f_k = 0.09$. We were able to capture this ablated particle (which had been exposed to three successive pulses, so it shows three damage craters) and image it using scanning electron microscopy. From the ratio of the diameter of the forward-facing crater to d, we estimate $m_a/m_0 \sim 0.013$, which is in reasonable agreement with the value (1.37%) calculated from the dynamics.

5. DISCUSSION

The data in Fig. 3(a) show that at a threshold value of $f_E E_0$, which depends on the particle diameter, the steady increase in $|v_0|$ suddenly turns into a drop. We attribute this to shattering of the particles, which will create sideways motion of fragments and reduce the amount of energy available for propulsion along the fiber axis. Below this threshold, however, it is interesting [Fig. 3(b)] that the proportion f_k of $f_E E_0$ that is converted to axial kinetic energy is almost independent of particle diameter. We attribute this to the size-independent numerical aperture of the ball-lens, which will make the focal spot diameter approximately independent of d so that f_k depends only on the total energy $f_E E_0$ incident on the particle. In other words, provided $f_E E_0$ is kept constant by increasing E_0 in inverse proportion to d^2, f_k will remain approximately constant. We can then write Eq. (2) as

$$v_0 = \frac{-2 f_k(f_E E_0) f_E E_0}{m_0 v_a}, \tag{5}$$

where $f_k(f_E E_0)$ is determined from the experimental data. It is approximately a piece-wise linear function, as shown by the thin black lines in Fig. 3(b) (the analytical expression is given in the caption).

A further intriguing aspect of Fig. 3(b) is that the response is separated into two distinct regimes, each with a different slope. Assuming that the field distribution at the focus is constant, the fraction of the focal area where the intensity exceeds the ablation threshold will initially increase with the energy incident on the particle. After the entire focal spot is ablated, any excess energy will be absorbed in the ablation plasma, increasing the kinetic energy, but at a smaller rate, as seen in the figure.

The measured values of v_0 are plotted in Fig. 4(a) versus d for center-core energy fluence $F_0 = 9.2$ and 4.6 nJ/μm^2 (open triangles and full lines). In both cases, v_0 is observed first to increase then saturate or decrease slightly. For $d = 0.8$ μm, the ball lens focuses only weakly (see Fig. 2) so that no ablation occurs. For $d = 1$ μm, the focusing was sufficient to induce ablation and backward particle motion, but only at the higher fluence value. At $d = 2$ μm, the focusing is optimal, the focal point lies within the particle, and the backward velocity reaches a maximum. For larger values of d, the focal point moves outside the particle, and v_0 saturates. Entering the piece-wise fit for $f_k(f_E E_0)$ from Fig. 3(b) into Eq. (5) plotting v_0, good agreement is obtained with the experimental measurements [full circles and dashed lines in Fig. 4(a)], despite the approximations of the model.

The volume within which the energy fluence is higher than some threshold value F_{th} can be estimated from the numerical simulations in Fig. 2(a), assuming that the energy fluence scales linearly with the power fluence in the vicinity of the focus. The best fit to the experimental results (see Supplement 1) is obtained for $F_{th} = 61$ nJ/μm^2, which is above the breakdown threshold (∼20 nJ/μm^2) for silica and well with the ablation range for sub-100 fs pulses [12]. Figure 2(b) plots the region where $|\mathbf{F}| > F_{th}$, keeping the total energy incident on the particles constant at 62.4 nJ for each particle diameter. We also note that the shape of the numerically calculated ablation crater for $d = 2.95$ μm is indeed similar to that seen in the SEM in Fig. 3(c). The smallest particle ($d = 0.8$ μm) is known to shatter at this incident pulse energy (Fig. 3), which is confirmed in Fig. 2(b), where we see that the ablation threshold is exceeded throughout the whole particle volume.

Next, we used the system to measure the viscous drag as a function of air pressure in the core. Exponential fits to the experimental data for a particle of diameter 2.78 μm and center-core energy fluence 4.6 nJ/μm^2 were used to calculate the decay constant γ and thus the value of η/C at five different pressures [open circles in Fig. 4(b)]. Under these conditions, the initial velocity $v_0 \sim -25$ m/s was approximately independent of pressure. Fits to aerosol theory [13] at three different temperatures [full curves in Fig. 4(b), see Supplement 1 for details] suggest that heating of the air may play a major role in determining the viscosity, which increases strongly with temperature. The results indicate that the air heats to around 800°K as a result of ionization of the glass. The ablation plasma will recombine over ns timescales, and the particle temperature will equalize over tens of nanoseconds [15], much more quickly than the timescale of particle motion. It may also be possible to operate at lower pressures, permitting particles to be displaced over greater distances, by using narrower cores to enhance the gradient forces at a given trapping power, and incorporating feedback to stabilize the transverse particle motion [16].

It is interesting to ask whether such high particle velocities will result in air turbulence. The Reynold's number $\mathrm{Re} = v_0 d/\nu = 33$ at $v_0 = 274$ m/s for particle diameter $d = 1.76$ μm, using the kinematic viscosity $\nu = 1.48 \times 10^{-5}$ m^2/s of ambient air (the influence of the hollow channel can be neglected since $D \gg d$). Although this value is intermediate between laminar and turbulent flow, the measured exponential time dependence of the velocity suggests that the flow is largely laminar. The value of Re at low pressures is difficult to predict since although the kinematic viscosity falls with pressure, it increases strongly with temperature.

Although backward rocket motion is superficially similar to "tractor beam" effects [17], the underlying physics is quite different, and the backward velocities are orders of magnitude higher. We also note that negative photophoretic effects induced by a continuous-wave laser beam have been used to propel absorbing particles backwards at speeds up to 10 cm/s [18], thousands of times smaller than what we report here; once again, the physics is quite different.

With further development, it should be possible to optimize the core diameter, pulse energy, duration, and chirp to accelerate

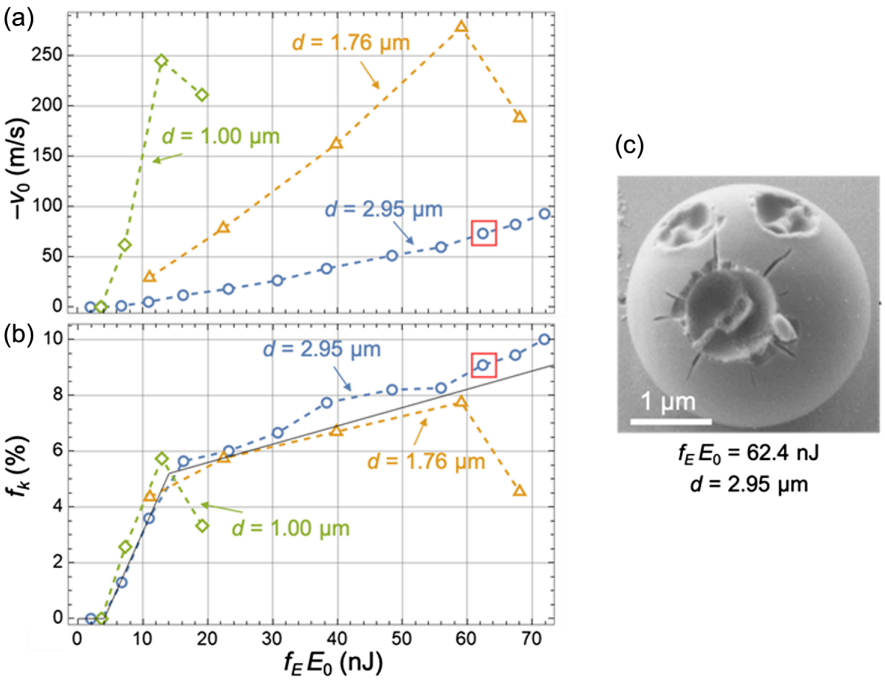

Fig. 3. Backward velocity and kinetic energy conversion factor versus incident energy. (a) Measured values of v_0 plotted against energy incident on the particle ($f_E E_0$) for particles with a diameter of 2.95 µm (circles), 1.76 µm (triangles), and 1.00 µm (diamonds). (b) The fraction f_k of the incident energy converted into kinetic energy (sum of backward and forward), plotted against $f_E E_0$. The thin black line is a stepwise linear fit to the data, defined as $f_k(q) = 0$ for $q < 4$, $0.52\,(q-4)$ for $3 < q < 14$ and $5.2 + 0.065(q-14)$ for $14 < q$, with q in nJ and f_k in %. (c) Scanning electron micrograph of a 2.95 µm particle after ablation by three pulses at $f_E E_0 = 62.4$ nJ [data points enclosed inside the red squares in (a) and (b); note that the data in (a) and (b) relate to the measured dynamics after incidence of the first pulse]. Note also the two-fold symmetric nanostructure in the damage craters, caused by the polarization dependence of the damage (Fig. 2).

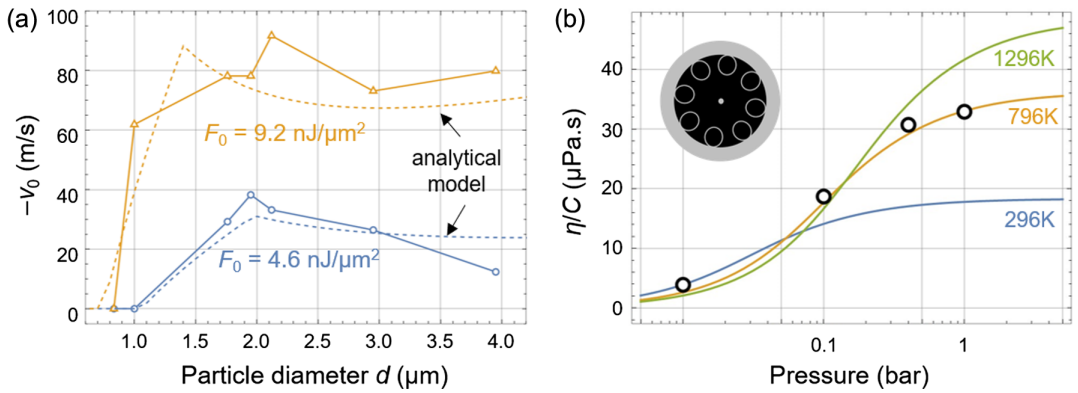

Fig. 4. Backwards velocity as a function of particle diameter and pressure dependence of viscosity. (a) Measured values of v_0 plotted versus d for center-core energy fluence $F_0 = 9.2$ and 4.6 nJ/µm^2 (open triangles and full lines). The dashed lines are based on Eq. (5) using the f_k function defined in the caption of Fig. 3. The fit is remarkably good, considering the model approximations. (b) Viscosity divided by the slip correction factor for a particle 2.78 µm in diameter (shown to scale in the inset), measured at different air pressures. The full curves are fits to aerosol theory Ref. [13] at three different temperatures, in which the Knudsen number is defined as the molecular mean free path divided by the particle diameter (see Supplement 1). The best fit to the experimental data is obtained at 796°K.

particles to high speed, while inflicting only minimal damage. It may be possible to reach higher velocities using a short burst of pulses at a high repetition rate, although of course, this will come at the cost of increasing particle damage. The technique may allow the inner walls of HC-PCF to be coated with a wide range of different materials at positions remote from the endfaces, shifting the anti-crossing wavelengths between the core mode and resonances in the core walls, and enabling incorporation of devices such as lasers, amplifiers, Bragg grating mirrors, and wavelength filters. In associated experiments, we observed femtosecond ablation for titania and vaterite particles, although as expected, the threshold value of $f_k E_0$ was different for each material (see Supplement 1). The use of counter-propagating fs pulses would prevent particle motion, enabling gradual build-up of a layer on the core wall at one position along the fiber. Longer pulses might be used to laser-evaporate particles without ionization, widening the range of possible materials.

In conclusion, ablation of micro-sized particles by single few-µJ femtosecond pulses accelerates the particles backwards at more than a million times g, causing rocket-like motion at initial

velocities approaching the speed of sound. The well-controlled micro-environment inside HC-PCF, together with transverse optical trapping, uniquely enables precise study of the post-ablation dynamics. The technique offers a novel means of coating the inner walls of HC-PCF with different materials.

Funding. Max-Planck-Gesellschaft.

Acknowledgment. We thank Amro Al-Khafaf for the help with finite element modelling, Eduard Butzen for making the SEM images, Martin Butryn for assistance with the laser system, and Sona Löwe for assistance in the graphics in Fig. 1.

Disclosures. The authors declare no conflicts of interest.

Data Availability. Data underlying the results presented in this paper are not publicly available at this time but may be obtained from the authors upon reasonable request.

Supplemental document. See Supplement 1 for supporting content.

REFERENCES

1. A. Ashkin, "Acceleration and trapping of particles by radiation pressure," Phys. Rev. Lett. **24**, 156–159 (1970).
2. K. C. Neuman and S. M. Block, "Optical trapping," Rev. Sci. Instrum. **75**, 2787–2809 (2004).
3. F. Benabid, J. C. Knight, and P. St.J. Russell, "Particle levitation and guidance in hollow-core photonic crystal fiber," Opt. Express **10**, 1195–1203 (2002).
4. D. S. Bykov, O. A. Schmidt, T. G. Euser, and P. St.J. Russell, "Flying particle sensors in hollow-core photonic crystal fibre," Nat. Photonics **9**, 461–465 (2015).
5. A. Sharma, S. Xie, R. Zeltner, and P. St.J. Russell, "On-the-fly particle metrology in hollow-core photonic crystal fibre," Opt. Express **27**, 34496–34504 (2019).
6. E. Mcleod and C. B. Arnold, "Subwavelength direct-write nanopatterning using optically trapped microspheres," Nat. Nanotechnol. **3**, 413–417 (2008).
7. R. Fardel, E. McLeod, Y.-C. Tsai, and C. B. Arnold, "Nanoscale ablation through optically trapped microspheres," Appl. Phys. A **101**, 41–46 (2010).
8. A. Shakhov, A. Astafiev, A. Gulin, and V. Nadtochenko, "Femtosecond nanostructuring of glass with optically trapped microspheres and chemical etching," ACS Appl. Mater. Interfaces **7**, 27467–27472 (2015).
9. H. Misawa, M. Koshioka, K. Sasaki, N. Kitamura, and H. Masuhara, "Three-dimensional optical trapping and laser ablation of a single polymer latex particle in water," J. Appl. Phys. **70**, 3829–3836 (1991).
10. S. Juodkazis and H. Misawa, "Controlled through-hole ablation of polymer microspheres," J. Micromech. Microeng. **14**, 1244–1248 (2004).
11. P. Uebel, M. C. Günendi, M. H. Frosz, G. Ahmed, N. N. Edavalath, J.-M. Ménard, and P. St.J. Russell, "Broadband robustly single-mode hollow-core PCF by resonant filtering of higher-order modes," Opt. Lett. **41**, 1961–1964 (2016).
12. I. Mirza, N. M. Bulgakova, J. Tomáštík, V. Michálek, O. Haderka, L. Fekete, and T. Mocek, "Ultrashort pulse laser ablation of dielectrics: thresholds, mechanisms, role of breakdown," Sci. Rep. **6**, 39133 (2016).
13. D. K. Hutchins, M. H. Harper, and R. L. Felder, "Slip correction measurements for solid spherical particles by modulated dynamic light scattering," Aerosol Sci. Technol. **22**, 202–218 (1995).
14. M. Lamperti, V. Jukna, O. Jedrkiewicz, P. Di Trapani, R. Stoian, T. E. Itina, C. Xie, F. Courvoisier, and A. Couairon, "Invited article: filamentary deposition of laser energy in glasses with Bessel beams," APL Photon. **3**, 120805 (2018).
15. R. R. Gattass and E. Mazur, "Femtosecond laser micromachining in transparent materials," Nat. Photonics **2**, 219–225 (2008).
16. J. Millen, T. S. Monteiro, R. Pettit, and A. N. Vamivakas, "Optomechanics with levitated particles," Rep. Prog. Phys. **83**, 026401 (2020).
17. W. Ding, T. Zhu, L.-M. Zhou, and C.-W. Qiu, "Photonic tractor beams: a review," Adv. Photon. **1**, 1 (2019).
18. J. Lin, A. G. Hart, and Y. Li, "Optical pulling of airborne absorbing particles and smut spores over a meter-scale distance with negative photophoretic force," Appl. Phys. Lett. **106**, 171906 (2015).